

Article

Effects of Reaction Temperature on the Photocatalytic Activity of TiO₂ with Pd and Cu Cocatalysts

Yu-Wen Chen *  and Yu-Hsuan Hsu

Department of Chemical and Materials Engineering, National Central University, Zhong-Li 32001, Taiwan; 107324032@cc.ncu.edu.tw

* Correspondence: ywchen@cc.ncu.edu.tw; Tel.: +886-3422-7151

Abstract: The aim of this study was to investigate the effects of reaction temperature on the photocatalytic activity of TiO₂ with Pd and Cu cocatalysts. N₂ sorption, transmission electron microscopy and high-resolution transmission electron microscopy were used to characterize the specific surface area, pore volume, pore size, morphology and metal distribution of the catalysts. The photocatalytic destruction of methylene blue under UV light irradiation was used to test its activity. The concentration of methylene blue in water was determined by UV-vis spectrophotometer. Pd/TiO₂ catalyst was more active than Cu/TiO₂ and TiO₂. At 0–50 °C reaction temperature, the activity of TiO₂ and Pd/TiO₂ increased with an increase of reaction temperature. When the temperature was as high as 70 °C, the reaction rate of TiO₂ drop slightly and Pd/TiO₂ became less effective. In contrast, Cu/TiO₂ was more active at room temperature than the other temperatures. The results indicate that the photocatalytic activity of the catalyst is influenced by the reaction temperature and the type of cocatalyst. When the reaction temperature is higher than 70 °C, the recombination of charge carriers will increase. The temperature range of 50–80 °C is regarded as the ideal temperature for effective photolysis of organic matter. The effects of reaction temperature mainly influence quantum effect, i.e., electron-hole separation and recombination.

Keywords: photocatalysis; titania; palladium; copper; reaction temperature effect



Citation: Chen, Y.-W.; Hsu, Y.-H. Effects of Reaction Temperature on the Photocatalytic Activity of TiO₂ with Pd and Cu Cocatalysts. *Catalysts* **2021**, *11*, 966. <https://doi.org/10.3390/catal11080966>

Academic Editors: Sami Rtimi, Dionysios (Dion) Demetriou, Dionysiou, Ewa Kowalska, Changseok Han and Marcin Janczarek

Received: 19 July 2021

Accepted: 10 August 2021

Published: 12 August 2021

Publisher's Note: MDPI stays neutral with regard to jurisdictional claims in published maps and institutional affiliations.



Copyright: © 2021 by the authors. Licensee MDPI, Basel, Switzerland. This article is an open access article distributed under the terms and conditions of the Creative Commons Attribution (CC BY) license (<https://creativecommons.org/licenses/by/4.0/>).

1. Introduction

TiO₂ has been used as a photocatalyst for many reactions. Many excellent reviews have been reported [1–16]. The advantages of TiO₂ are high chemical stability, non-toxicity and low cost [17–37]. Pd, Ag and Cu et al. have been used as the cocatalysts of TiO₂ by facilitating electron transfer and therefore inhibiting electron-hole recombination, as well as by improving the photocatalytic response under the visible region [21,22,26–34]. However, most of the studies on photocatalytic reaction were carried out at room temperature [17–37]. In contrast, there are very few works focused on the effect of temperature on the photocatalytic reaction [38–44]. It has been known that reaction temperature can influence the photocatalytic reaction rate. This is particularly important since around 50% of the overall solar energy that reaches Earth's surface is derived from the infrared band of the spectrum, which is perceived as heat [16].

Barakat et al. [38] reported the effects of the temperature on the photodegradation process using Ag-doped TiO₂ nanostructures. They reported that the increase in the temperature has positive impact on the photocatalytic activity of Ag/TiO₂ and the highest degradation rate was at 55 °C. In contrast, in the case of the nanofibrous morphology, the temperature has negative effect and the optimum temperature was 25 °C. It shows the increase of temperature resulted in increase the kinetic energy of the dye molecules, so the molecules escape from the active thin film surrounding the photocatalyst. Kim et al. [39] investigated the effect of reaction temperature (298–353 K) on photocatalytic H₂ production in bare and Pt/TiO₂ suspensions containing Ethylenediaminetetraacetic acid (EDTA).

H₂ production rates increased by ~7.8- and ~2.5-fold in TiO₂ and Pt/TiO₂, respectively, from 298 K to 323 K. It shows the positive relationship between reaction temperature 298 and 323 K. The charge carrier mobility and interfacial charge transfer improves at higher temperatures. The photocatalytic degradation of organic components over the TiO₂/sepiolite composites at different temperatures were investigated [40]. It shows that, the reaction temperature can influence the photocatalytic activity of the catalyst and the optimum temperature was 50 °C. Mateo et al. [41] gave an excellent review on photo-thermal catalysis. Through the synergistic combination of photo- and thermo-chemical contributions of sunlight, photo-thermal catalysis can enhance reaction rates. The temperature effect is mainly due to the localized surface plasmon resonance. However, the mechanism of reaction temperature on the photocatalytic activity is complicate and remains unclear.

The aim of this study was to investigate the effects of reaction temperature on the photocatalytic activity of TiO₂ with Pd and Cu cocatalysts in the destruction of organic dye. It is believed that the reaction temperature would influence the photocatalytic properties of TiO₂ with Pd and Cu cocatalysts, since electron-hole separation and recombination are influenced by the reaction temperature, and different cocatalysts would have different effects.

2. Results and Discussion

2.1. X-ray Diffraction (XRD)

The XRD patterns of the samples are shown in Figure 1. Only anatase and rutile phases were detected. The peak positions are the same among all samples, indicating that adding metals did not change the crystalline phases of TiO₂. No XRD peaks for Pd and Cu were detected, indicating that Pd and Cu metal particles were very less than 4 nm.

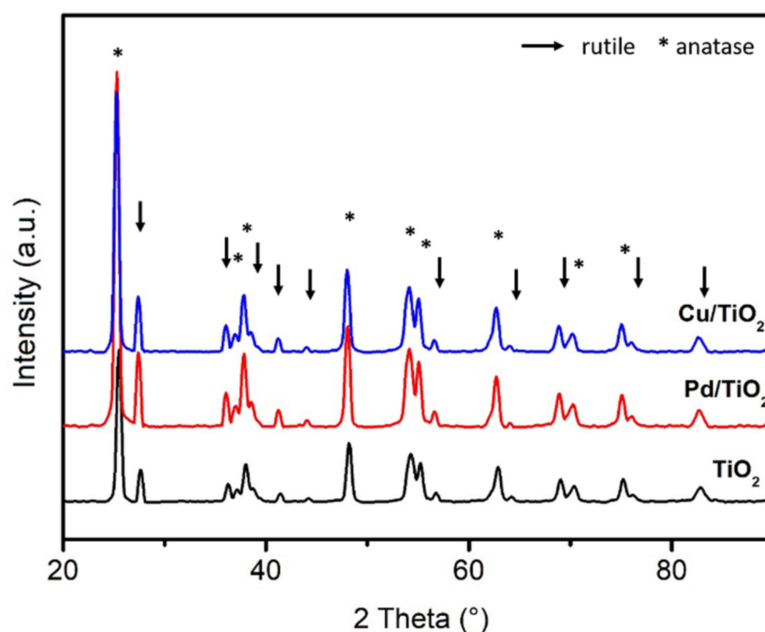


Figure 1. The XRD patterns of the catalysts.

2.2. Pore Structure of the Catalyst

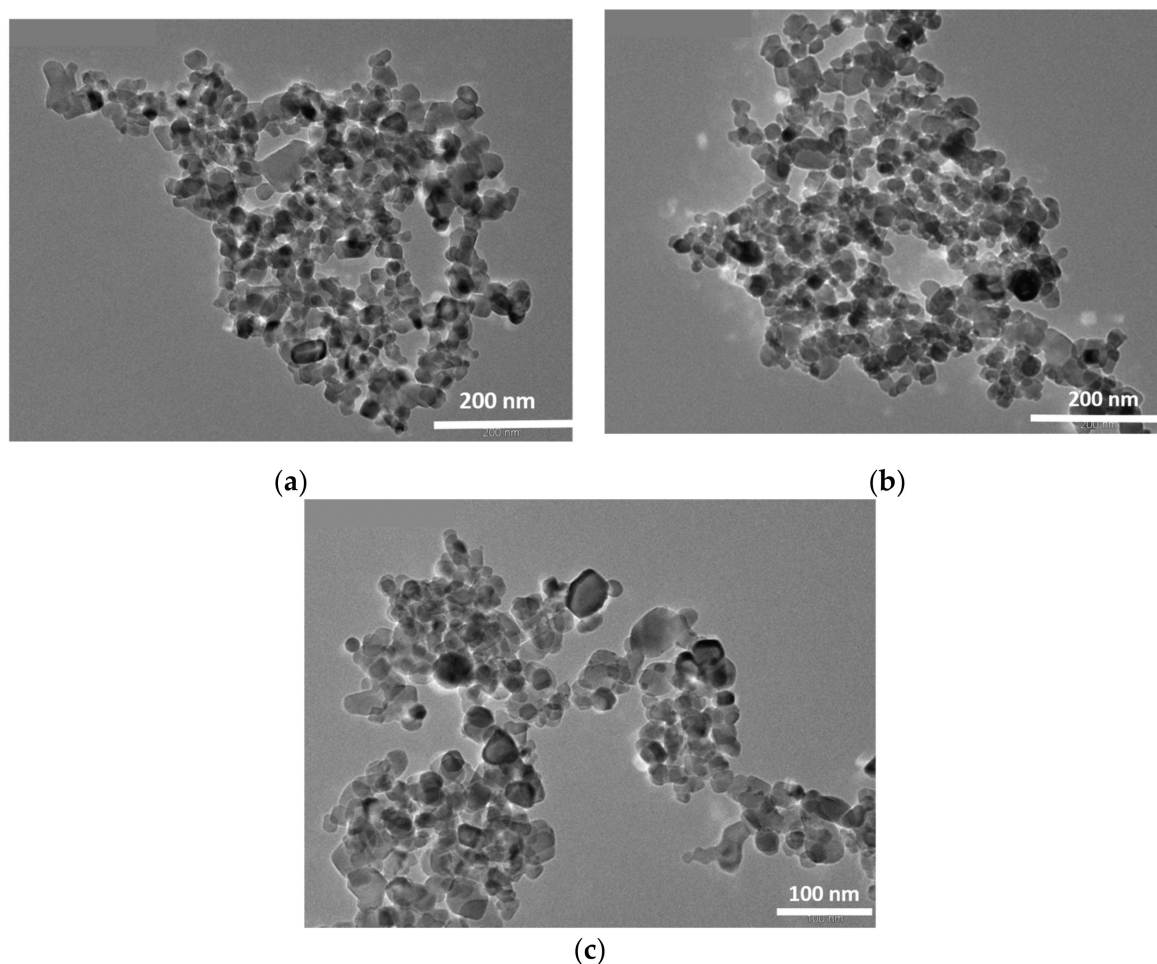
Table 1 shows the surface area and pore structure of the samples. Since the commercial TiO₂ was used as the catalyst, adding small amount of metal did not change the pore structure significantly, as expected.

Table 1. The physical properties of Pd/TiO₂ and pure TiO₂.

Sample	BET Surface Area (m ² /g)	Desorption Average Pore Diameter (Å)	BJH Cumulative Volume of Pores (cm ³ /g)	BJH Average Pore Width (Å)
TiO ₂	51.3	283	0.364	236.0
Pd/TiO ₂	50.6	293	0.372	242.4
Cu/TiO ₂	48.6	309	0.377	253.7

2.3. Transmission Electron Microscopy (TEM)

The TEM images of the samples are shown in Figure 2. TiO₂ did not change its morphology after metal deposition. However, due to the low resolution of TEM, we were not able to see the clear picture of the metals. It infers that the metal particles were very small. HR-TEM was used in the further study.

**Figure 2.** The TEM images of (a) TiO₂, (b) Pd/TiO₂, (c) Cu/TiO₂.

2.4. High-Resolution Transmission Electron Microscopy (HRTEM) and Energy-Dispersive X-ray Spectroscopy (EDS)

HRTEM images of the Pd/TiO₂ and Cu/TiO₂ are shown in Figure 3. Very small nano metal particles were observed. The particle sizes of Pd and Cu metals were about 2 nm and were homogeneously distributed on the surface of TiO₂. The results are consistent with the XRD results.

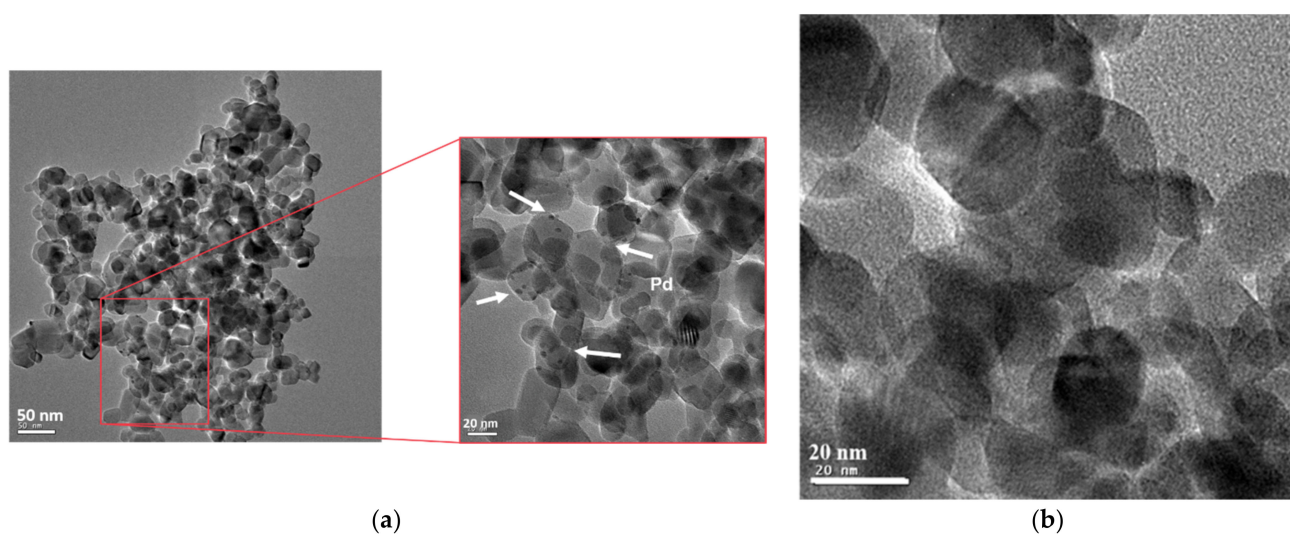


Figure 3. HRTEM images of (a) Pd/TiO₂ and (b) Cu/TiO₂.

The EDS mapping of each element on Pd/TiO₂ are shown in Figure 4. It clearly shows that Pd metal particles were homogeneously distributed on the surface of TiO₂, in consistent with HR-TEM result. Figure 5 shows the EDS mapping of each element on Cu/TiO₂. Cu metal particles were also homogeneously distributed on the surface of TiO₂. The EDS results also show that the Pd and Cu metal loadings are 0.498 wt.% and 0.506 wt.%, respectively. The real metal loadings are the same as the nominal loadings within experimental error. Since the catalysts were prepared by incipient-wetness impregnation, it is very easy to have the same metal loading as that in the precursor.

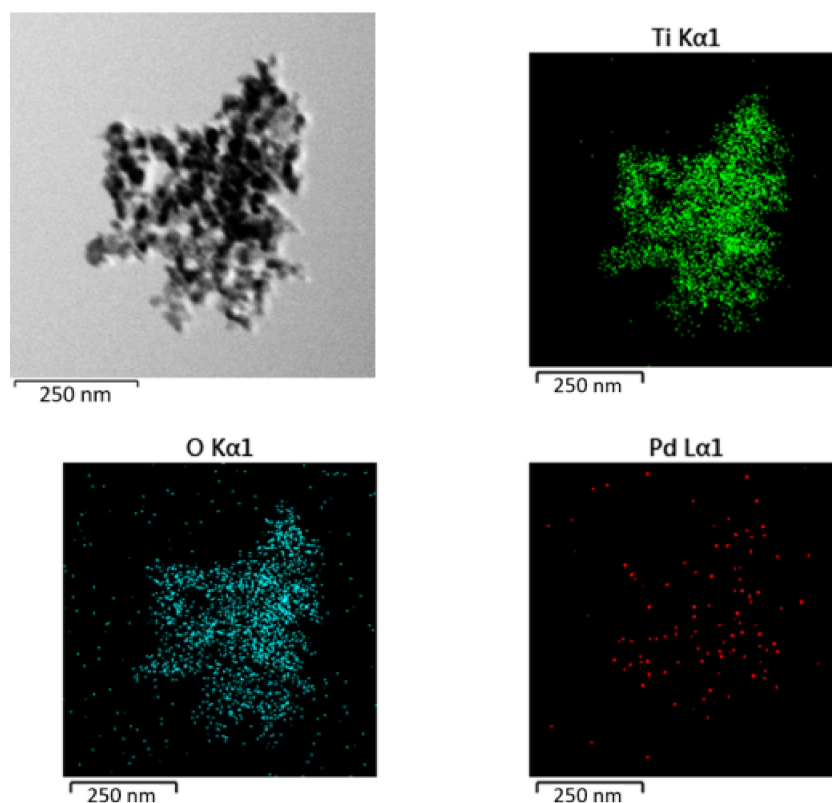


Figure 4. EDS element mapping image of Pd/TiO₂ sample.

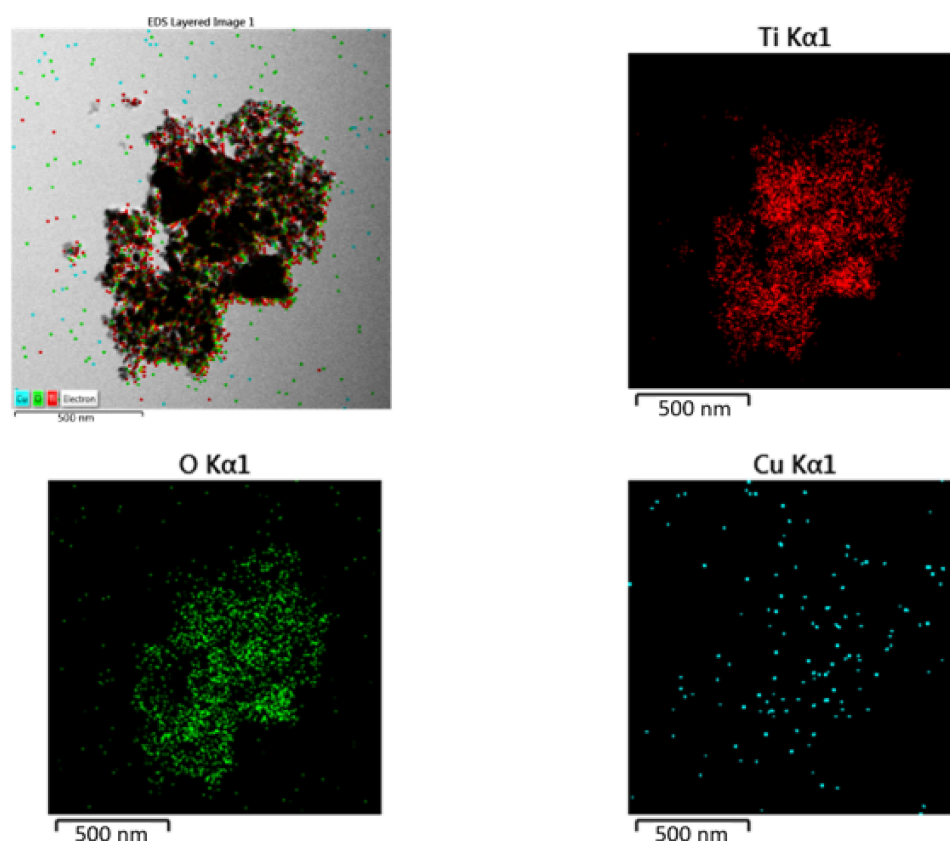


Figure 5. EDS element mapping image of Cu/TiO₂.

2.5. Photocatalytic Reaction

Figure 6 shows the concentration of methylene blue vs. time on TiO₂ at various reaction temperatures. Some of methylene blue was adsorbed on TiO₂. Figure 7a shows the results of the C/C_0 of bare TiO₂ vs. reaction temperature, where C is the concentration of methylene blue and C_0 is the initial concentration of methylene blue. It shows that the activity at 50 °C was higher than those at other temperature. It can be noted that when the reaction temperature was 0 °C, the reaction rate was very low. It has been known from the literature that when the temperature is lower, the solubility of methylene blue in the water is lower [42]. This may cause partial condensation of methylene blue in water.

Kumar et al. [43] reported that when the reaction temperature is higher than 80 °C, the recombination of charge carriers will increase. The temperature range of 20–80 °C is regarded as the ideal temperature for effective photolysis of organic matter. In their study, four reaction temperatures were tested, i.e., 0 °C, 25 °C, 50 °C and 70 °C. They reported that the higher the temperature is, the higher the reaction rate is of TiO₂. When the temperature reaches 70 °C, the reaction rate drops slightly. Our results are in accord. It has been reported that the photocatalytic activity of TiO₂ increased as the reaction temperature increased. In the study of Parra et al. [44], the TiO₂ (P25) was tested at 20, 40, 55 and 70 °C, respectively. Their results are in line with this study.

Figure 7b shows that the kinetic studies of the degradation of methylene blue over the TiO₂ obtained at different temperatures. The summary of the pseudo-first-order kinetics of the as-prepared samples under UV light irradiation is shown in Table 2. From Figure 7b, it is plausible to suggest that the photocatalytic degradation reactions of methylene blue on the catalyst followed the pseudo-first-order reaction according to the Langmuir–Hinshelwood (LH) model and may be expressed as [17,19,26,28,44,45]:

$$\ln(C_0/C) = kt \quad (1)$$

where k is the apparent reaction rate constant, C_0 is the initial concentration of methylene blue and C is the concentration of methylene blue at the reaction time t . The results of rate constants of TiO_2 at different reaction temperature are tabulated in Table 2.

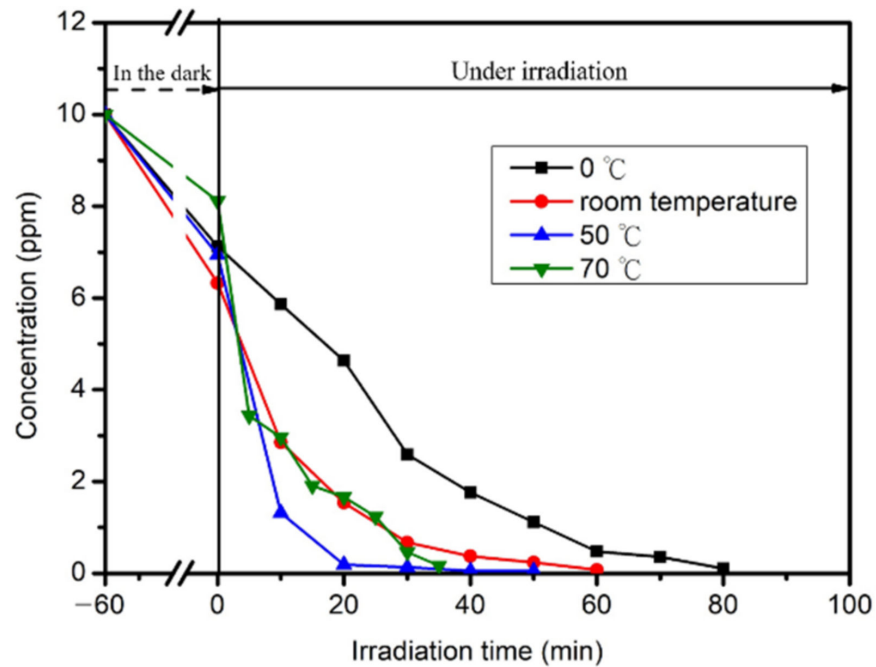


Figure 6. The change of the concentration of methylene blue on TiO_2 with time at different reaction temperatures.

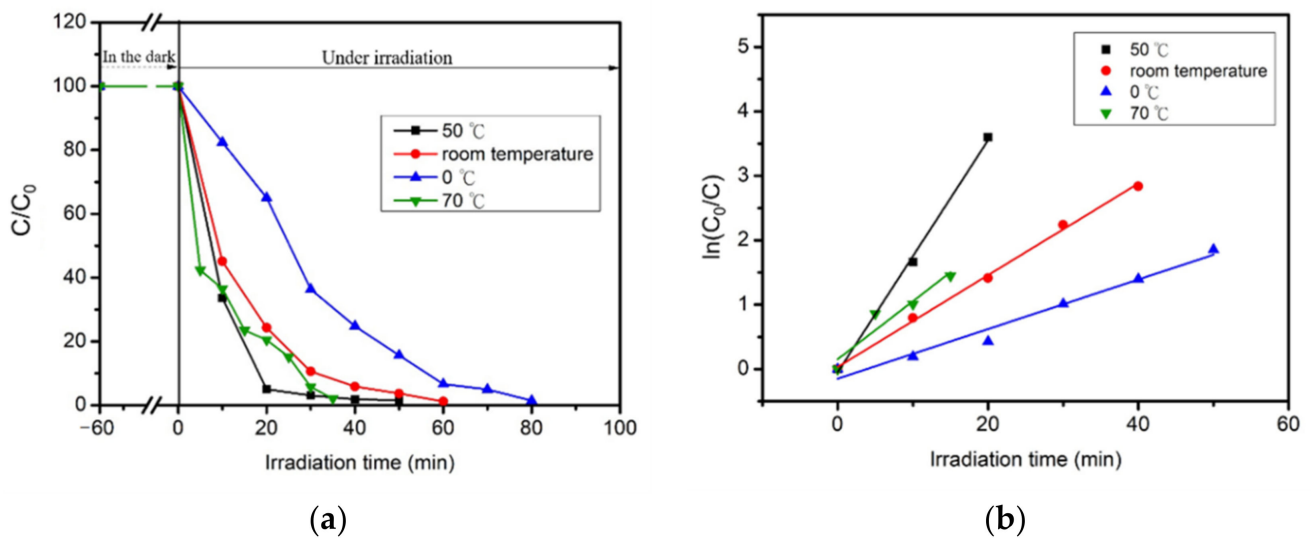


Figure 7. (a) Photodegradation of bare TiO_2 at different reaction temperatures; (b) photocatalytic activities of TiO_2 at different reaction temperatures by plotting $\ln(C_0/C)$ versus irradiation time (min).

Table 2. Rate constants of reactions of the samples at different reaction temperatures.

As-Prepared Powder	Reaction Temperature (°C)	Rate Constant (k, min ⁻¹)
TiO ₂	0	0.00309
TiO ₂	25	0.07122
TiO ₂	50	0.17998
TiO ₂	70	0.08986
Pd/TiO ₂	0	0.07874
Pd/TiO ₂	25	0.1114
Pd/TiO ₂	50	0.29942
Pd/TiO ₂	70	0.04893
Cu/TiO ₂	0	0.04677
Cu/TiO ₂	25	0.07321
Cu/TiO ₂	50	0.05428

Figure 8 shows the concentration of methylene blue vs. irradiation time on Pd/TiO₂. It shows that higher amount of methylene blue was adsorbed on Pd/TiO₂, compared with TiO₂. It infers that Pd also can adsorb methylene blue in dark. Figure 9a shows the activities of Pd/TiO₂ at various temperatures. At 0–50 °C, the higher reaction temperature is, the higher the reaction rate is. As the reaction temperature increases, the movement of photoelectron-hole pairs becomes more active, electrons can combine with adsorbed oxygen faster and holes can generate OH radicals together with -OH faster [46–48], thereby improving the degradation efficiency of methylene blue. However, when the reaction temperature raised to 70 °C, the activity became low. This is because that adsorption is an exothermic reaction, while desorption is an endothermic reaction. Figures 6 and 8 show that the adsorption capacity of Pd/TiO₂ is greater than that of TiO₂. When the temperature reached 70 °C, methylene blue desorbs faster from Pd/TiO₂ than that from TiO₂. After 35 min, the degradation rate of TiO₂ was as high as 98%, but it is obvious that the original white TiO₂ was blue-violet color, which proves that most of the methylene blue was adsorbed on TiO₂. Comparing with TiO₂, the color of Pd/TiO₂ after degradation was the same as that of the original catalyst. It shows that Pd/TiO₂ was very active at 50 °C. The rate constant of methylene blue degradation on Pd/TiO₂ can be extracted from Figure 9b and listed in Table 2. It shows that Pd/TiO₂ was much active than TiO₂. By elevating the reaction temperature from 25 to 50 °C, the photocatalytic activity increased, because charge carrier mobility and interfacial charge transfer improves at higher temperatures. Further increase the temperature to 70 °C, the activity decreased since the electron-hole recombination rate increased. Various cocatalysts, such as Pd and Cu, have been used as the cocatalyst of TiO₂ [49–55]. The cocatalyst can suppress electron-hole recombination rate and resulted in longer life time of electron and hole and higher photocatalytic activity. Different cocatalyst has different influence on the electron-hole recombination rate. Reaction temperature also plays a crucial role on the recombination rate. Ghasemi et al. [56] accessed the thermodynamic parameters of activation. However, they only calculate the activation energy in the range of positive relationship between activity and reaction temperature. A blank test of reaction was carried out at various temperatures without catalyst. It did not have any degradation of methylene blue. Therefore, the effects of reaction temperature mainly influence quantum effect, i.e., electron-hole separation and recombination. Further research is needed to elucidate this quantum effect.

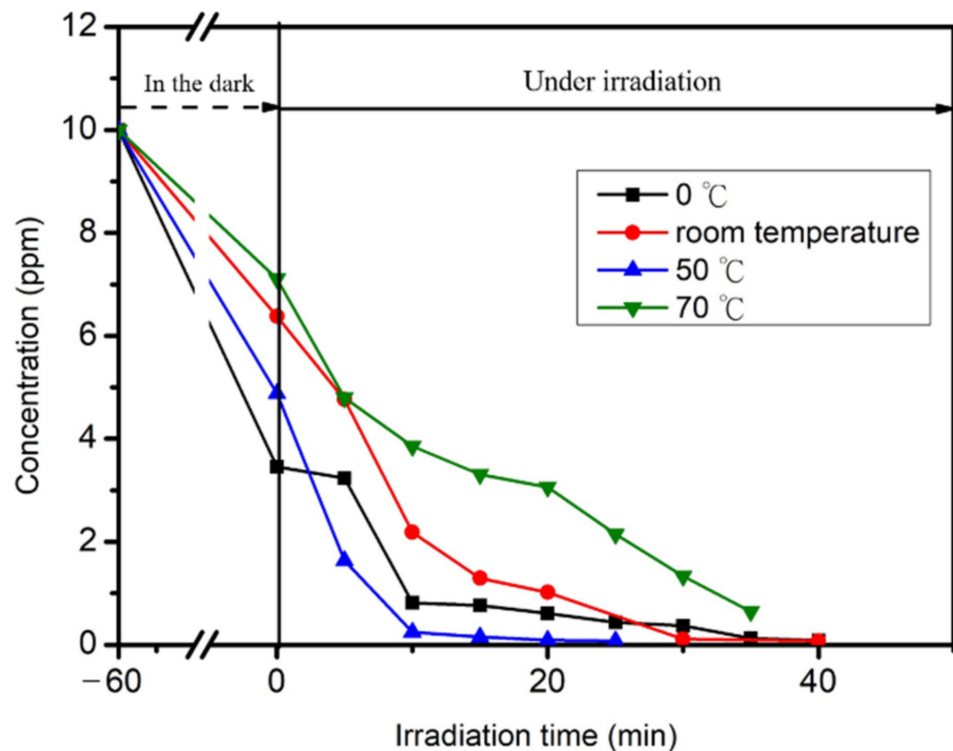


Figure 8. The change of the concentration of methylene blue on Pd/TiO₂ with time at different reaction temperatures.

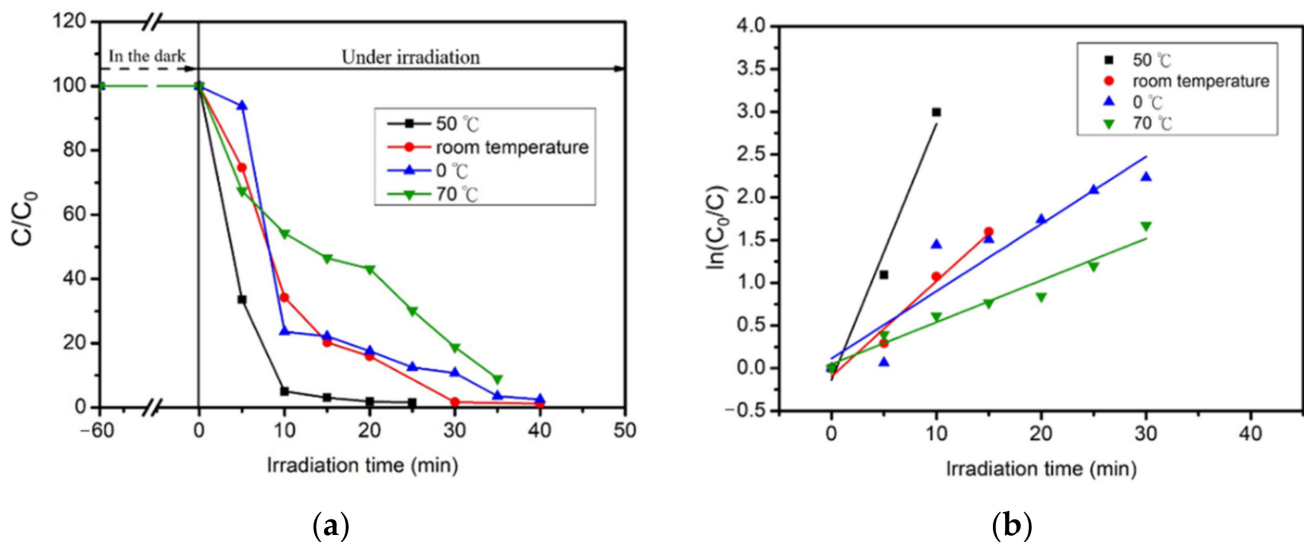


Figure 9. (a) Photodegradation of Pd/TiO₂ at different reaction temperatures; (b) Photocatalytic activities of Pd/TiO₂ at different reaction temperatures by plotting $\ln(C_0/C)$ versus irradiation time (min).

Figure 10 shows the concentration of methylene blue vs. irradiation time at different temperatures on Cu/TiO₂. Figure 11 shows the C/C_0 of methylene blue on Cu/TiO₂ at different reaction temperatures. The activity of Cu/TiO₂ is different from those of bare TiO₂ and Pd/TiO₂. Cu/TiO₂ has the highest reaction rate at room temperature than at the other temperatures. In the study of Meng et al. [46], a copper-containing photocatalytic material was prepared, and tested for photodegradation of Rhodamin B. At the reaction temperatures of 15, 25, 35 and 45 °C, it had the highest activity at 45 °C. In particular, it also shows that the activity at 25 °C is higher than that at 35 °C. Meng et al. [46] reported

that the increase of the reaction temperature more strongly promotes the movement of the dye molecules so that the dye molecules can more easily penetrate the micropores of the material. However, when the reaction temperature continues to rise, the degradation efficiency of dye reached equilibrium. It can be seen that when the reaction temperature rises to a certain value, the effect of reaction temperature on the photocatalytic activity is small [46]. Our results show that Cu/TiO₂ had low photocatalytic activity at 0 °C. The activity increased at 25 °C and 50 °C. There is a little difference in activity between 0 °C and 50 °C.

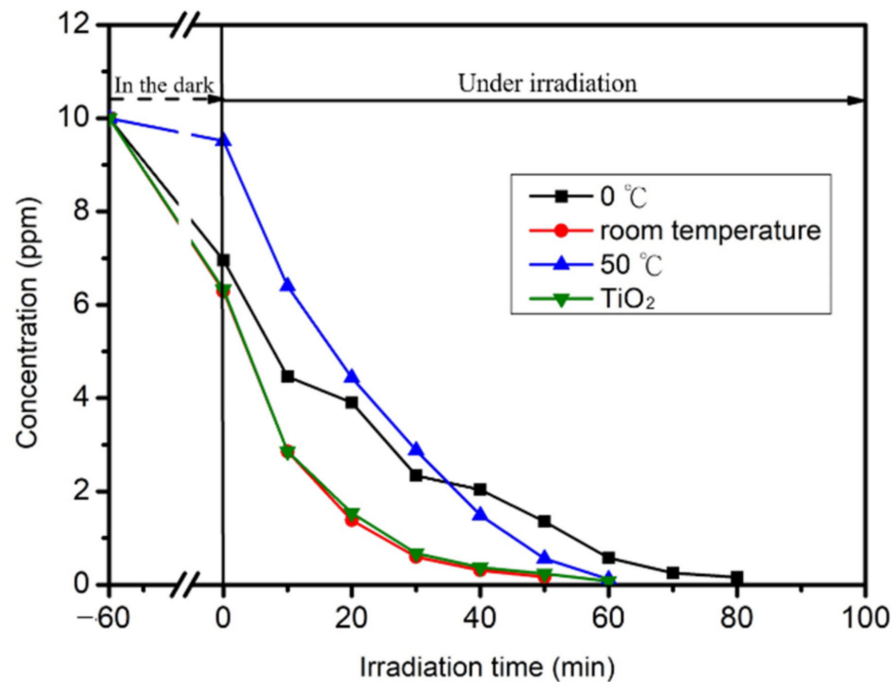


Figure 10. The change of the concentration of methylene blue on Cu/TiO₂ with time at different reaction temperatures.

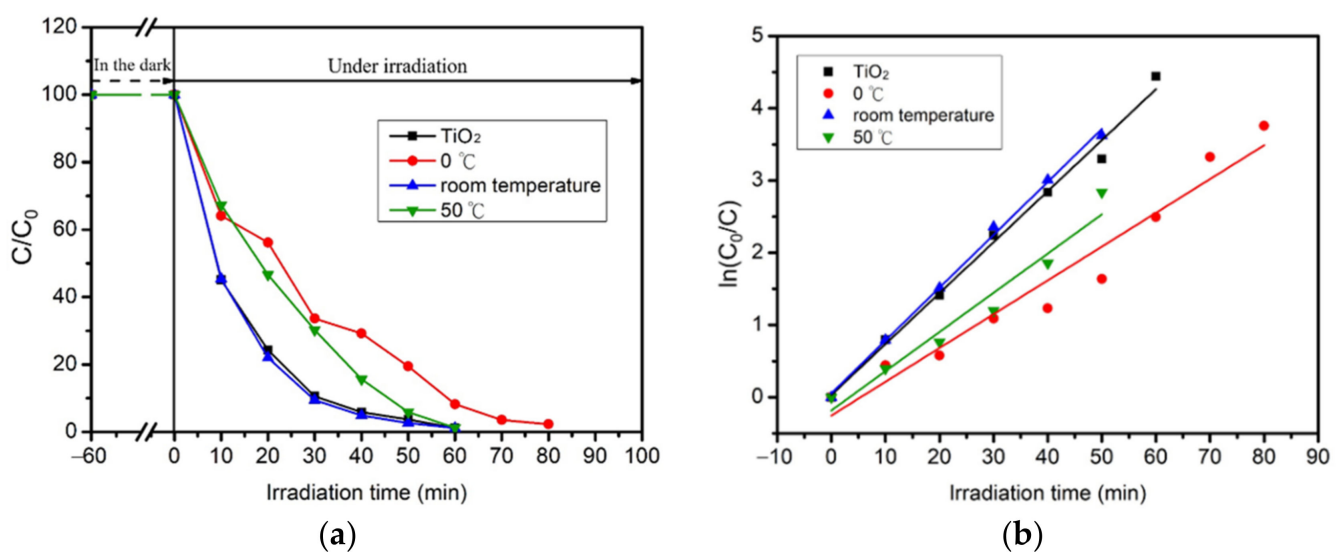


Figure 11. (a) Photodegradation of Cu/TiO₂ at different reaction temperatures; (b) Photocatalytic activities of Cu/TiO₂ at different reaction temperatures by plotting $\ln(C_0/C)$ versus irradiation time (min).

Comparing the reaction rates of Pd/TiO₂ and Cu/TiO₂ under the most suitable conditions (Table 2), the photocatalytic activity of Pd/TiO₂ was much greater than that of

Cu/TiO₂ and that of Cu/TiO₂ was slightly greater than that of TiO₂ at 25 °C. The effects of reaction temperature on the catalyst are varied by the type of cocatalyst.

3. Materials and Methods

3.1. Materials

Titanium dioxide (P25) was purchased from Evonik Degussa, Essen, Germany. Copper nitrate and palladium nitrate were purchased from Sigma-Aldrich, Merck KGaA, Darmstadt, Germany. Methylene blue was purchased from Alfa Aesar, Lancashire, United Kingdom.

3.2. Catalysts Preparation

Pd/TiO₂ and Cu/TiO₂ were prepared by incipient-wetness impregnation method according to the following procedure. First, metal nitrate was dissolved in 1 mL distilled water to form an aqueous solution. It was slowly added in TiO₂ powder. The impregnated sample was dried under vacuum for 3 h. The sample was illuminated under UV light for 1 day. The metal loading of the sample was 0.5 wt.%

3.3. Catalysts Characterization

3.3.1. Pore Structure of the Catalyst

N₂ sorption was used to measure the specific surface area and pore structure of the sample. The BET (Brunauer-Emmet-Teller) method was used to measure specific surface area and pore volume. The average pore size and its distribution were estimated from the desorption isotherm by Barrette-Joynere-Halenda (BJH) analysis.

3.3.2. Transmission Electron Microscopy (TEM) and High-Resolution Transmission Electron Microscopy (HRTEM)

The morphologies, dispersive effect and particle sizes of the samples were determined by the TEM, JEOL, Tokyo, Japan, JEM-2000 FX II. HRTEM was operated on a JEOL JEM-2010 operated at 200 kV. A small amount of sample was put into a sample bottle filled with distilled water and agitated under an ultrasonic environment for 1 h. One drop of the dispersed slurry was dipped onto a carbon-coated nickel mesh (200 #; Ted Pella Inc., Altadena, CA, USA), and dried in the vacuum oven at 65 °C overnight to remove the water entirely. The chemical composition of the samples and the interaction of the metals were determined by Energy-dispersive X-ray spectroscopy (EDS) attached on the HRTEM. The HRTEM (JEOL JEM-F200, Tokyo, Japan) images were recorded digitally by a Gatan slow-scan camera (GIF) (AMETEK, Berwyn, PA, USA).

3.4. Photocatalytic Reaction

For the photocatalytic activity reaction, the catalyst was activated for 12 h by two UVC lamps (Philips, Eindhoven Holland, wavelength = 254 nm, TUV PL-L 18W/4P 1CT/25). 20 mL of methylene blue aqueous solution with a concentration of 10 mg/L was loaded in a beaker. Before performing the photocatalytic activity reaction, the reactor was kept in the dark for 1 h to reach saturated adsorption of methylene blue. The reaction temperature was varied by a heating plate through the separate water bath, using two UVC lamps from top to bottom illumination. The concentration of methylene blue in aqueous solution was determined every 5 min by a UV/Visible/NIR Spectrophotometer (Hitachi, Tokyo, Japan, U-4100). The wavelength for the measurement was 663 nm, which is the maximum characterized adsorption wavelength of methylene blue.

4. Conclusions

The effects of reaction temperature on the photocatalytic activity of TiO₂ with Pd and Cu cocatalysts were investigated in this study. At 0–50 °C reaction temperature, the activity of TiO₂ and Pd/TiO₂ increased with an increase of reaction temperature. When the temperature was as high as 70 °C, the reaction rate of TiO₂ drop slightly, and Pd/TiO₂

became less effective. In contrast, Cu/TiO₂ was more active at room temperature than the other temperatures.

Comparing the reaction rates of Pd/TiO₂ and Cu/TiO₂ under the most suitable conditions, the catalytic activity of Pd/TiO₂ is much greater than that of Cu/TiO₂, and that of Cu/TiO₂ is slightly greater than that of TiO₂. The effects of reaction temperature on the catalyst are varied by the type of cocatalyst. When the reaction temperature is higher than 70 °C, the recombination of charge carriers will increase. The temperature range of 50–80 °C is regarded as the ideal temperature for effective photolysis of organic matter. The effects of reaction temperature mainly influence quantum effect, i.e., electron-hole separation and recombination.

Author Contributions: Conceptualization, Y.-W.C.; methodology, Y.-H.H.; formal analysis, Y.-H.H.; investigation, Y.-H.H.; writing—original draft preparation, Y.-W.C.; writing—review and editing, Y.-H.H. All authors have read and agreed to the published version of the manuscript.

Funding: This research was funded by Ministry of Science and Technology, Taiwan, grant number MOST-110-2221-E008-009.

Institutional Review Board Statement: Not applicable.

Informed Consent Statement: Not applicable.

Data Availability Statement: Not applicable.

Conflicts of Interest: The authors declare no conflict of interest. The funders had no role in the design of the study; in the collection, analyses or interpretation of data; in the writing of the manuscript or in the decision to publish the results.

References

1. Petersen, T.; Klüner, T. Photodesorption of H₂O from anatase-TiO₂ (101): A combined quantum chemical and quantum dynamical study. *J. Phys. Chem. C* **2020**, *124*, 11444–11455. [[CrossRef](#)]
2. Liu, B.; Wu, H.; Parkin, I.P. New insights into the fundamental principle of semiconductor photocatalysis. *ACS Omega* **2020**, *5*, 14847–14856. [[CrossRef](#)]
3. Gao, C.; Low, J.; Long, R.; Kong, T.; Zhu, J.; Xiong, Y. Heterogeneous single-atom photocatalysts: Fundamentals and applications. *Chem. Rev.* **2020**, *120*, 12175–12216. [[CrossRef](#)]
4. Leong, S.; Razmjou, A.; Wang, K.; Hapgood, K.; Zhang, X.; Wang, H. TiO₂ based photocatalytic membranes: A review. *J. Membr. Sci.* **2014**, *472*, 167–184. [[CrossRef](#)]
5. Rahimi, N.; Pax, R.A.; Gray, E.M.A. Review of functional titanium oxides. I: TiO₂ and its modifications. *Prog. Solid State Chem.* **2016**, *44*, 86–104. [[CrossRef](#)]
6. Abdullah, H.; Khan, M.M.R.; Ong, H.R.; Yaakob, Z. Modified TiO₂ photocatalyst for CO₂ photocatalytic reduction: An overview. *J. CO₂ Util.* **2017**, *22*, 15–32. [[CrossRef](#)]
7. Ibhaddon, A.; Fitzpatrick, P. Heterogeneous photocatalysis: Recent advances and applications. *Catalysts* **2013**, *3*, 189–218. [[CrossRef](#)]
8. Linsebigler, A.L.; Lu, G.; Yates, J.T. Photocatalysis on TiO₂ Surfaces: Principles, Mechanisms, and Selected Results. *Chem. Rev.* **1995**, *95*, 735–758. [[CrossRef](#)]
9. Liu, L.; Chen, X. Titanium dioxide nanomaterials: Self-structural modifications. *Chem. Rev.* **2014**, *114*, 9890–9918. [[CrossRef](#)]
10. Nakata, K.; Fujishima, A. TiO₂ photocatalysis: Design and applications. *J. Photochem. Photobiol. C Photochem. Rev.* **2012**, *13*, 169–189. [[CrossRef](#)]
11. Magalhães, P.; Andrade, L.; Nunes, O.C.; Mendes, A. Titanium dioxide photocatalysis: Fundamentals and application on photoinactivation. *Rev. Adv. Mater. Sci.* **2017**, *51*, 91–129.
12. Pawar, M.; Sendoğdular, S.; Gouma, P. A brief overview of TiO₂ photocatalyst for organic dye remediation: Case study of reaction mechanisms involved in Ce-TiO₂ photocatalysts system. *J. Nanomater.* **2018**, *2018*, 5953609. [[CrossRef](#)]
13. Wold, A. Photocatalytic properties of titanium dioxide (TiO₂). *Chem. Mater.* **1993**, *5*, 280–283. [[CrossRef](#)]
14. Basavarajappa, P.S.; Patil, S.B.; Ganganagappa, N.; Reddy, K.R.; Raghu, A.V.; Reddy, C.V. Recent progress in metal-doped TiO₂, non-metal doped/codoped TiO₂ and TiO₂ nanostructured hybrids for enhanced photocatalysis. *Int. J. Hydrogen Energy* **2020**, *45*, 7764–7778. [[CrossRef](#)]
15. Noman, M.T.; Ashraf, M.A.; Ali, A. Synthesis and applications of nano-TiO₂: A review. *Environ. Sci. Pollut. Res.* **2019**, *26*, 3262–3291. [[CrossRef](#)]
16. Schneider, J.; Matsuoka, M.; Takeuchi, M.; Zhang, J.; Horiuchi, Y.; Anpo, M.; Bahnemann, D.W. Understanding TiO₂ photocatalysis: Mechanisms and materials. *Chem. Rev.* **2014**, *114*, 9919–9986. [[CrossRef](#)]

17. Harris, J.; Silk, R.; Smith, M.; Dong, Y.; Chen, W.T.; Waterhouse, G.I.N. Hierarchical TiO₂ nanoflower photocatalysts with remarkable activity for aqueous methylene blue photo-oxidation. *ACS Omega* **2020**, *5*, 18919–18934. [[CrossRef](#)] [[PubMed](#)]
18. AlSalka, Y.; Al-Madanat, O.; Curti, M.; Hakki, A.; Bahnemann, D.W. Photocatalytic H₂ Evolution from Oxalic Acid: Effect of Cocatalysts and Carbon Dioxide Radical Anion on the Surface Charge Transfer Mechanisms. *ACS Appl. Energy Mater.* **2020**, *3*, 6678–6691. [[CrossRef](#)]
19. Nath, R.R.; Nethravathi, C.; Rajamathi, M. Hierarchically porous, biphasic, and C-Doped TiO₂ for solar photocatalytic degradation of dyes and selective oxidation of benzyl alcohol. *ACS Omega* **2021**, *6*, 12124–12132. [[CrossRef](#)]
20. Pinedo-Escobar, J.F.; Fan, F.; Moctezuma, E.; Gomez-Solis, C.; Martinez, C.J.C.; Gracia-Espino, E. Nanoparticulate double-heterojunction photocatalysts comprising TiO₂(anatase)/WO₃/TiO₂(rutile) with enhanced photocatalytic activity toward the degradation of methyl orange under near-ultraviolet and visible Light. *ACS Omega* **2021**, *6*, 11840–11848. [[CrossRef](#)]
21. GÜnnemann, C.; Bahnemann, D.W.; Robertson, P.K.J. Isotope effects in photocatalysis: An underexplored issue. *ACS Omega* **2021**, *6*, 11113–11121. [[CrossRef](#)]
22. Yaemsunthorn, K.; Kobielski, M.; Macyk, W. TiO₂ with tunable anatase-to-rutile nanoparticles ratios: How does the photoactivity depend on the phase composition and the nature of photocatalytic reaction? *ACS Appl. Nano Mater.* **2021**, *4*, 633–643. [[CrossRef](#)]
23. Zhao, C.; Zhou, L.; Zhang, Z.; Gao, Z.; Weng, H.; Zhang, W.; Li, L.; Song, Y.Y. Insight of the influence of magnetic-field direction on magneto-plasmonic interfaces for tuning photocatalytic performance of semiconductors. *J. Phys. Chem. Lett.* **2020**, *11*, 9931–9937. [[CrossRef](#)]
24. Sangpour, P.; Hashemi, F.; Moshfegh, A.Z. Photoenhanced degradation of methylene blue on cosputtered M: TiO₂ (M: Au, Ag, Cu) nanocomposite systems: A comparative study. *J. Phys. Chem. C* **2010**, *114*, 13955–13961. [[CrossRef](#)]
25. Rismanchian, A.; Chen, Y.W.; Chuang, S.S.C. In situ infrared study of photoreaction of ethanol on Au and Ag/TiO₂. *Catal. Today* **2016**, *264*, 16–22. [[CrossRef](#)]
26. Moongraksathum, B.; Hsu, P.T.; Chen, Y.W. Photocatalytic activity of ascorbic acid-modified TiO₂ sol prepared by the peroxo sol–gel method. *J. Sol Gel Sci. Technol.* **2016**, *78*, 647–659. [[CrossRef](#)]
27. Moongraksathum, B.; Lee, D.S.; Chen, Y.W. Monodispersibility and size control in the preparation of spherical titania particles by thermal hydrolysis of TiCl₄ in various solvents. *J. Taiwan Inst. Chem. Eng.* **2016**, *68*, 455–460. [[CrossRef](#)]
28. Moongraksathum, B.; Chen, Y.W. CeO₂–TiO₂ mixed oxide thin films with enhanced photocatalytic degradation of organic pollutants. *J. Sol. Gel. Sci. Technol.* **2017**, *82*, 772–782. [[CrossRef](#)]
29. Moongraksathum, B.; Chen, Y.W. Anatase TiO₂ co-doped with silver and ceria for antibacterial application. *Catal. Today* **2018**, *310*, 69–74. [[CrossRef](#)]
30. Moongraksathum, B.; Shang, J.Y.; Chen, Y.W. Photocatalytic antibacterial effectiveness of Cu-doped TiO₂ thin film prepared via peroxo sol–gel method. *Catalysts* **2018**, *8*, 352. [[CrossRef](#)]
31. Moongraksathum, B.; Chien, M.Y.; Chen, Y.W. Antiviral and antibacterial effects of silver-doped TiO₂ prepared by the peroxo sol–gel method. *J. Nanosci. Nanotechnol.* **2019**, *19*, 7356–7362. [[CrossRef](#)]
32. Tseng, H.C.; Chen, Y.W. Facile synthesis of Ag/TiO₂ by Photoreduction method and its degradation activity of methylene blue under UV and visible light irradiation. *Mod. Res. Catal.* **2020**, *9*, 97149. [[CrossRef](#)]
33. Shang, J.Y.; Chen, Y.W. Photoactivity of CuO–TiO₂ nanocomposite photocatalyst under twilight irradiation. *Curr. Top. Catal.* **2020**, *14*, 97–110.
34. Wu, J.Y.; Chen, Y.W. Preparation of WO₃-modified TiO₂ thin film by peroxo sol–gel method and its photocatalytic activity in degradation of methylene blue. *Res. Chem. Intermed.* **2020**, *46*, 4627–4643. [[CrossRef](#)]
35. Tseng, H.C.; Chen, Y.W. Surface modification of TiO₂ by silver incorporation and its photocatalytic activity under twilight irradiation. *Trends Photochem. Photobiol.* **2020**, *19*, 23–34.
36. Wu, J.Y.; Chen, Y.W. Anticorrosion of WO₃-modified TiO₂ thin film prepared by peroxo sol–gel method. *Mod. Res. Catal.* **2020**, *9*, 35–46. [[CrossRef](#)]
37. Chen, Y.W.; Tsai, K.J. Anatase TiO₂ co-doped with silver and silica for destruction of organic dye and bacteria. *J. Sol. Gel. Sci. Technol.* **2021**, *97*, 651–662. [[CrossRef](#)]
38. Barakat, N.A.M.; Kanjwal, M.A.; Chronakis, I.S.; Kim, H.Y. Influence of temperature on the photodegradation process using Ag-doped TiO₂ nanostructures Negative impact with the nanofibers. *J. Mol. Catal. A Chem.* **2013**, *366*, 333–340. [[CrossRef](#)]
39. Kim, G.; Choi, H.J.; Kim, H.; Kim, J.; Monllor-Satoca, D.; Kim, M.; Park, H. Temperature-boosted photocatalytic H₂ production and charge transfer kinetics on TiO₂ under UV and visible light. *Photochem. Photobiol. Sci.* **2016**, *15*, 1247–1253. [[CrossRef](#)] [[PubMed](#)]
40. Zhang, Y.; Wang, D.; Zhang, G. Photocatalytic degradation of organic contaminants by TiO₂/sepiolite composites prepared at low temperature. *Chem. Eng. J.* **2011**, *173*, 1–10. [[CrossRef](#)]
41. Nakano, K.; Obuchi, E.; Nanri, M. Thermo-photocatalytic decomposition of acetaldehyde over Pt–TiO₂/SiO₂. *Chem. Eng. Res. Des.* **2004**, *82*, 297–301. [[CrossRef](#)]
42. Salimi, A.; Roosta, A. Experimental solubility and thermodynamic aspects of methylene blue in different solvents. *Thermochim. Acta* **2019**, *675*, 134–139. [[CrossRef](#)]
43. Kumar, A.; Pandey, G. A Review on the factors affecting the photocatalytic degradation of hazardous materials. *Mater. Sci. Eng. Int. J.* **2017**, *1*, 106–114.

44. Parra, S.; Stanca, E.S.; Guasaquillo, I.; Thampi, R.K. Photocatalytic degradation of atrazine using suspended and supported TiO₂. *Appl. Catal. B Environ.* **2014**, *51*, 107–116. [[CrossRef](#)]
45. Mateo, D.; Cerrillo, J.L.; Durini, S.; Gascon, J. Fundamentals and applications of photo-thermal catalysis. *Chem. Soc. Rev.* **2021**, *50*, 2173–2210. [[CrossRef](#)] [[PubMed](#)]
46. Meng, Y.; Xia, S.; Pan, G.; Xue, J.; Jiang, J.; Ni, Z. Preparation and photocatalytic activity of composite metal oxides derived from Salen-Cu(II) intercalated layered double hydroxides. *Korean J. Chem. Eng.* **2017**, *34*, 2331–2341. [[CrossRef](#)]
47. Yamamoto, A.; Mizuno, Y.; Kentaro Teramura, K.; Shishido, T.; Tanaka, T. Effects of reaction temperature on the photocatalytic activity of photo-SCR of NO with NH₃ over a TiO₂ photocatalyst. *Catal. Sci. Technol.* **2013**, *3*, 1771–1775. [[CrossRef](#)]
48. Ojstršek, A.; Kleinschek, K.S.; Fakin, D. Characterization of nano-sized TiO₂ suspensions for functional modification of polyester fabric. *Surf. Coat. Technol.* **2013**, *226*, 68–74. [[CrossRef](#)]
49. Liu, E.; Qi, L.; Bian, J.; Chen, Y.; Hu, X.; Fan, J.; Liu, H.; Zhu, C.; Wang, Q. A facile strategy to fabricate plasmonic Cu modified TiO₂ nano-flower films for photocatalytic reduction of CO₂ to methanol. *Mater. Res. Bull.* **2015**, *68*, 203–209. [[CrossRef](#)]
50. Orudzhev, F.F.; Isaev, A.B.; Shabanov, N.S.; Gasanova, F.G.; Idrisova, A.K.; Babaeva, D.P. Photoelectrocatalytic oxidation of phenol on silver loaded TiO₂ nanotube array at high oxygen pressure under luminescent light irradiation. *Int. J. Electrochem. Sci.* **2018**, *13*, 4548–4560. [[CrossRef](#)]
51. Lacerda, A.M.; Larrosa, I.; Dunn, S. Plasmon enhanced visible light photocatalysis for TiO₂ supported Pd nanoparticles. *Nanoscale* **2015**, *7*, 12331–12335. [[CrossRef](#)] [[PubMed](#)]
52. Orudzhev, F.F.; Gasanova, F.G.; Aliev, Z.M.; Isaev, A.B. Photoelectrocatalytic oxidation of phenol on platinum-modified TiO₂ nanotubes. *Nanotechnol. Russ.* **2012**, *7*, 482–485. [[CrossRef](#)]
53. Esmat, M.; El-Hosainy, H.; Tahawy, R.; Jevasuwan, W.; Tsunoji, N.; Fukata, N.; Ide, Y. Nitrogen doping-mediated oxygen vacancies enhancing co-catalyst-free solar photocatalytic H₂ production activity in anatase TiO₂ nanosheet assembly. *Appl. Catal. B Environ.* **2021**, *285*, 119755. [[CrossRef](#)]
54. Doustkhah, E.; Assadi, M.H.N.; Komaguchi, K.; Tsunoji, N.; Esmat, M.; Fukata, N.; Tomita, O.; Abe, R.; Ohtani, B.; Ide, Y. In situ Blue titania via band shape engineering for exceptional solar H₂ production in rutile TiO₂. *Appl. Catal. B Environ.* **2021**, *297*, 120380–120392. [[CrossRef](#)]
55. Esmat, M.; Farghali, A.A.; El-Dek, S.I.; Khedr, M.H.; Yamauchi, Y.; Bando, Y.; Fukata, N.; Ide, Y. Conversion of a 2D Lepidocrocite-type layered titanate into its 1D nanowire form with enhancement of cation exchange and photocatalytic performance. *Inorg. Chem.* **2019**, *58*, 7989–7996. [[CrossRef](#)]
56. Ghasemi, Z.; Younesi, H.; Zinatizadeh, A.A. Kinetics and thermodynamics of photocatalytic degradation of organic pollutants in petroleum refinery wastewater over nano-TiO₂ supported on Fe-ZSM-5. *J. Taiwan Inst. Chem. Eng.* **2016**, *65*, 357–366. [[CrossRef](#)]